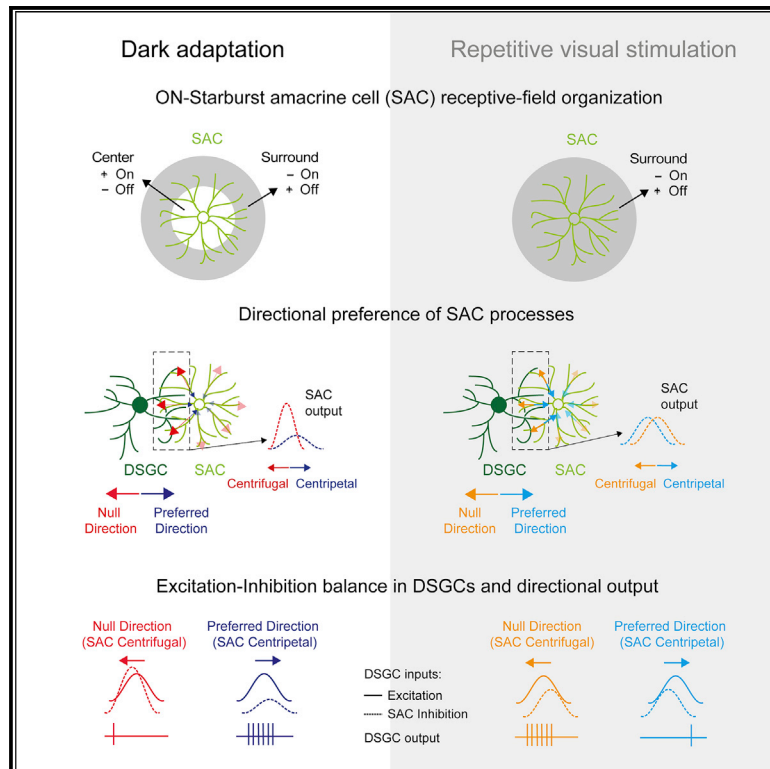


# Antagonistic Center-Surround Mechanisms for Direction Selectivity in the Retina

## Graphical Abstract



## Authors

Lea Ankri, Elishai Ezra-Tsur,  
Shir R. Maimon, Nathali Kaushansky,  
Michal Rivlin-Etzion

## Correspondence

michal.rivlin@weizmann.ac.il

## In Brief

Ankri et al. uncover a functional role for antagonistic center-surround receptive field organization in retinal direction selectivity. Stimulation of a starburst amacrine cell's center and surround elicits temporally distinct responses, thereby supporting the computation of opposite motion directions in direction-selective ganglion cells.

## Highlights

- Repetitive visual stimulation eliminates center and boosts surround response in SAC
- Changes in center-surround abolish SAC direction selectivity and shift its response
- Shifted SAC responses alter inhibition timing and reverse DSGC directional tuning
- SAC center and surround elicit directional responses in DSGC to opposite directions



## Report

# Antagonistic Center-Surround Mechanisms for Direction Selectivity in the Retina

Lea Ankri,<sup>1</sup> Elishai Ezra-Tsur,<sup>1,2</sup> Shir R. Maimon,<sup>1</sup> Nathali Kaushansky,<sup>1,3</sup> and Michal Rivlin-Etzion<sup>1,4,\*</sup><sup>1</sup>Department of Neurobiology, Weizmann Institute of Science, Rehovot 76100, Israel<sup>2</sup>Department of Mathematics and Computer Science, The Open University of Israel, Ra'anana, Israel<sup>3</sup>Present address: Department of Immunology, Weizmann Institute of Science, Rehovot 76100, Israel<sup>4</sup>Lead Contact\*Correspondence: [michal.rivlin@weizmann.ac.il](mailto:michal.rivlin@weizmann.ac.il)<https://doi.org/10.1016/j.celrep.2020.107608>

## SUMMARY

An antagonistic center-surround receptive field is a key feature in sensory processing, but how it contributes to specific computations such as direction selectivity is often unknown. Retinal On-starburst amacrine cells (SACs), which mediate direction selectivity in direction-selective ganglion cells (DSGCs), exhibit antagonistic receptive field organization: depolarizing to light increments and decrements in their center and surround, respectively. We find that a repetitive stimulation exhausts SAC center and enhances its surround and use it to study how center-surround responses contribute to direction selectivity. Center, but not surround, activation induces direction-selective responses in SACs. Nevertheless, both SAC center and surround elicited direction-selective responses in DSGCs, but to opposite directions. Physiological and modeling data suggest that the opposing direction selectivity can result from inverted temporal balance between excitation and inhibition in DSGCs, implying that SAC's response timing dictates direction selectivity. Our findings reveal antagonistic center-surround mechanisms for direction selectivity and demonstrate how context-dependent receptive field reorganization enables flexible computations.

## INTRODUCTION

To achieve spatial acuity, sensory systems are required to employ computational motifs that enable delicate sampling of the environment. Such is center-surround receptive field organization, which is present at all levels of visual processing and is considered a key mechanism for the enhancement of edge detection and color vision. On cells depolarize to light increments in the center of their receptive fields, but are inhibited by light increments in their surround. In addition, On cells frequently exhibit Off-surround activation: a depolarizing response to a dark stimulus in the periphery (Barlow, 1953; Kuffler, 1953). Off cells display a similar antagonism with opposite polarity preference. Despite the prevalence of this receptive field organization, little is known about its impact on the various visual modalities encoded by the retina. For example, starburst amacrine cells (SACs), retinal interneurons that underlie direction selectivity, display antagonistic center-surround organization, but whether and how this organization contributes to direction selectivity is poorly understood.

On-Off direction-selective ganglion cells (DSGCs) respond maximally to motion in their preferred direction (PD) and minimally to motion in the opposite, null direction (ND). SACs mediate this directional response via asymmetric wiring: only processes oriented in the DSGC's ND tend to form GABAergic inhibitory synapses on the DSGC (Figure 1A; Briggman et al., 2011). Although SACs do not show directional preference to

linear motion at the soma level, each SAC process is itself direction selective, responding with greater depolarization to motion away from the cell soma (centrifugal [CF]) than to motion toward cell soma (centripetal [CP]) (Ding et al., 2016; Euler et al., 2002; Fransen and Borghuis, 2017; Koren et al., 2017). Due to their wiring specificity, SAC processes that innervate a given DSGC display directional preference to the DSGCs' ND (Figure 1A), which is expected to result in stronger GABA release during null than during preferred motion. This asymmetric inhibition is thought to play a crucial role in direction selectivity.

SAC center-surround organization results from its inputs arrangement. Its center responses are derived from excitatory inputs that are confined to its proximal two-thirds dendritic arbors. This organization is thought to contribute to SAC CF preference (Ding et al., 2016; Vlasits et al., 2016). In addition, reciprocal SAC-SAC lateral inhibition enhances CF preference (Lee and Zhou, 2006; Zhou and Lee, 2008), but this surround inhibition is not strictly required because blocking GABA receptors fails to fully eliminate SACs' directional responses (Chen et al., 2016; Hanson et al., 2019; Hausselt et al., 2007; Oesch and Taylor, 2010). Although the role of SAC surround in direction selectivity was tested by abolishing their surround responses, it was never assessed by abolishing center responses.

We previously showed that a short repetitive visual stimulation (RVS) switches SAC's polarity preference (Vlasits et al., 2014), and that a subset of DSGCs can also reverse their directional



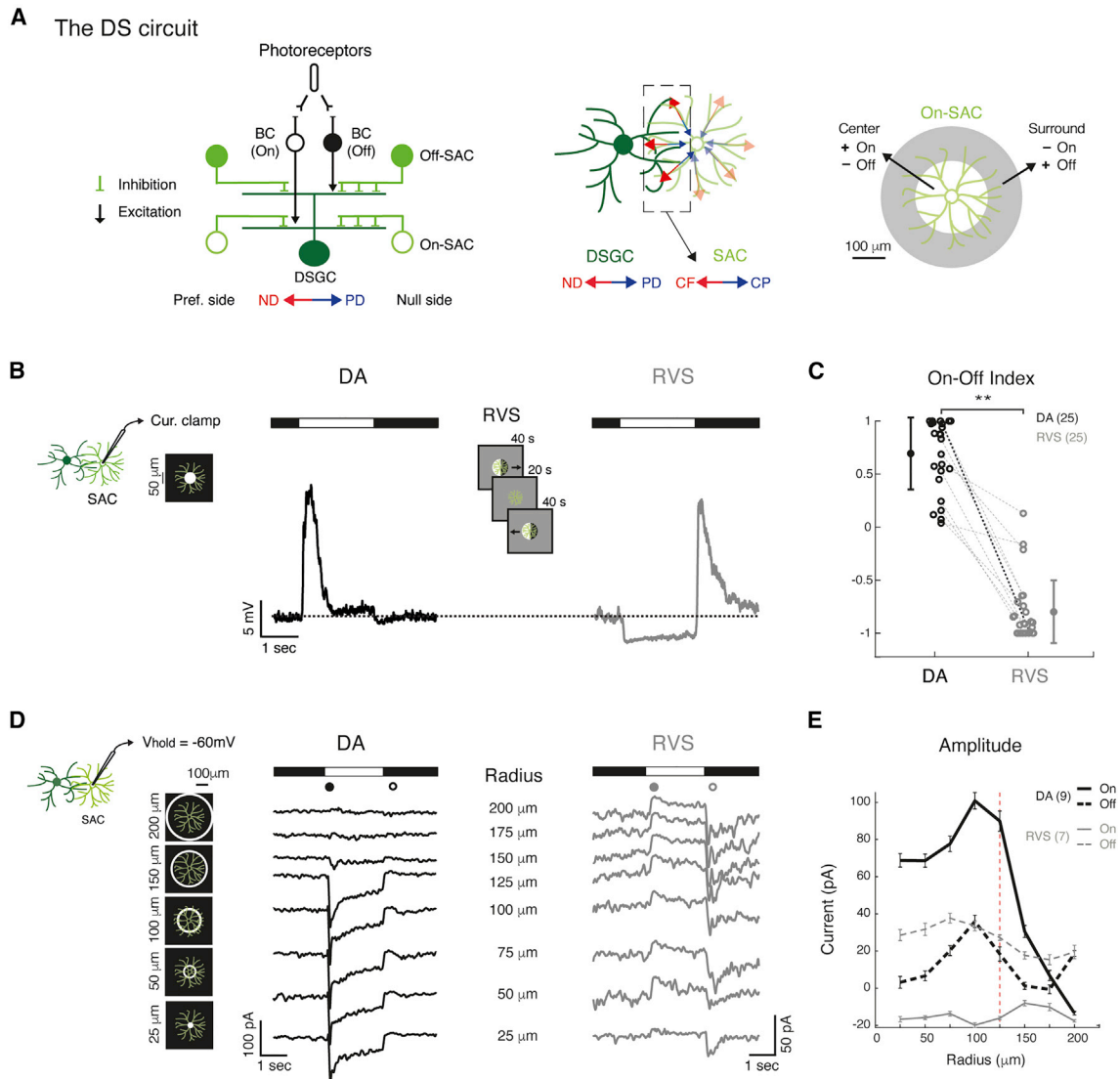


**Figure 1. RVS Reorganizes SAC Center-Surround Receptive Field**

(A) Left: schematics of the direction-selective (DS) circuit, side view. Middle: a DSGC with one innervating SAC, top view. Dashed box denotes SAC processes that are oriented in the DSGC's ND, providing it with GABAergic inhibition. Right: On-SAC antagonistic center-surround organization.

(B) Average current-clamp recordings of an example On-SAC in response to a 2-s bright spot (50-μm radius) in dark-adapted (DA; black) conditions and following RVS (gray). RVS is illustrated in the center. Dashed line denotes the baseline voltage.

(C) On-Off index of On-SACs in DA conditions and following RVS. Dashed lines connect values of the same cell; bold line represents the cell in (B). Group means and SD are indicated on the side by circles and error bars.

(D) Average voltage-clamp recordings ( $V_{\text{hold}} = -60$  mV) from an example On-SAC in response to 2-s static rings of eight different radii (specified in the center; five are illustrated on the left), in DA conditions and following RVS. Black and gray dots denote the periods used for the population analysis in (E).

(E) Maximal amplitude (mean  $\pm$  SEM) of the excitatory currents as a function of ring radius in DA conditions and following RVS for light onset and offset (continuous and dashed lines, respectively). Dashed vertical line denotes the distal boundary of SAC excitatory receptive field.

For all panels, asterisks indicate statistical significance (\* $p < 0.05$ ; \*\* $p < 0.005$ ). Numbers of cells in each group are in brackets. BC, bipolar cell; CF, centrifugal; CP, centripetal; ND, null direction; PD, preferred direction.

preference following the same stimulation (Rivlin-Etzion et al., 2012). Here, we employ this RVS to shed light on the contribution of SACs to retinal direction selectivity in its original and reversed form. We show that SAC polarity switch occurs because of reorganization of its receptive field following RVS, which abolishes center and enhances surround responses. Although

RVS-evoked changes abolished SAC CF preference, both center-mediated (assessed prior to RVS) and surround-mediated responses (assessed following RVS) prompted directional responses in DSGC: center activation elicited responses to the PD, whereas surround activation elicited responses to the ND. These opposed direction responses could be explained

by a change in SAC response timing. Thus, SAC receptive field organization can affect DSGC computation by controlling both the timing and amount of inhibition, implying a motif of center-surround antagonism in the retinal direction-selective circuit, in which PD motion is encoded in the center receptive field and ND motion in the surround.

## RESULTS

### On-SACs Lose Center and Enhance Surround Responses following RVS

We have previously shown that a RVS with drifting gratings in the timescale of minutes can switch the polarity of excitatory inputs to SACs in the dorsal retina (Vlasits et al., 2014). Here, we confirmed these results using current-clamp recordings, demonstrating that On-SACs depolarize to the onset of a bright spot in dark-adapted (DA) conditions, but depolarize to the spot's disappearance following RVS (Figures 1B and 1C; Figure S1). Because this switch in polarity preference matches surround-mediated responses, we suspected that RVS changes SAC receptive field organization. To examine this, we recorded SAC excitatory currents while stimulating them with static rings of different radii (25–200  $\mu\text{m}$ ). DA On-SACs revealed excitatory inputs at ring onset, which increased with ring radius, reaching a maximum value in response to a  $\sim 100\text{-}\mu\text{m}$  radius and rapidly decreasing in response to larger ring radii (Figures 1D and 1E). These findings match SACs' restriction of glutamatergic inputs to the inner two-thirds of the dendritic tree (Ding et al., 2016; Vlasits et al., 2016). A portion of the DA SACs revealed surround activation at ring offset (Figures 1E; Figure S1A), which could result from disinhibition of On bipolar cells mediated by wide-field amacrine cells (Lee and Zhou, 2006). Following RVS, however, On-SAC excitation emerged solely in response to the ring's offset and was independent of ring radius, indicating a loss of the characteristic proximal excitation to light onset and center-surround organization (Figures 1D and 1E; one-way ANOVA, On:  $p_{\text{DA}} < 0.001$ ,  $p_{\text{RVS}} = 0.26$ ; Off:  $p_{\text{DA}} < 0.05$ ,  $p_{\text{RVS}} = 0.29$ ). Moreover, DA SACs exhibited robust responses to proximal stimulation and more modest responses to full-field stimulation, whereas following RVS, responses to full-field stimulation were more robust than responses to proximal stimulation (Figures S1B and S1C). This change in SAC receptive field following RVS implies an enhancement of surround over center response and probably results from activation of surround circuits in the outer retina (see Discussion).

### On-SACs Lose Their Directional Preference and Shift Their Responses following RVS

Because SAC proximal excitation is thought to contribute to their CF preference (Ding et al., 2016; Vlasits et al., 2016), its loss may affect SAC directional preference. To test this, we stimulated On-SACs with expanding (CF motion) and collapsing (CP motion) drifting rings centered on the cell's soma while recording SAC somatic voltage. In accordance with previous reports, DA On-SACs tended to display stronger depolarization in response to CF than to CP motion (Figures 2A and 2B, top; Ding

et al., 2016; Euler et al., 2002; Fransen and Borghuis, 2017; Koren et al., 2017). This CF preference was reflected by a positive annular direction-selective index (A-DSI; see STAR Methods;  $\text{A-DSI}_{\text{DA}} = 0.19 \pm 0.2$ ; Figure 2C) and a shorter rise time to CF motion (see STAR Methods;  $\text{rt}_{\text{DA\_CF}} = 75 \pm 38$  ms,  $\text{rt}_{\text{DA\_CP}} = 162 \pm 71$  ms;  $p < 0.001$ ; Figure 2D).

Following RVS, On-SAC response asymmetries disappeared, revealing similar voltage waveforms during CF and CP motion (Figures 2A and 2B, bottom). This resulted in reduced A-DSI values, which clustered around zero ( $\text{A-DSI}_{\text{RVS}} = 0.01 \pm 0.09$ ;  $\text{A-DSI}_{\text{DA}}$  versus  $\text{A-DSI}_{\text{RVS}}$ :  $p < 0.001$ ; Figure 2C), and similar rise times ( $\text{rt}_{\text{RVS\_CF}} = 77 \pm 34$  ms,  $\text{rt}_{\text{RVS\_CP}} = 95 \pm 29$  ms;  $p = 0.19$ ; Figure 2D). On-SAC enhanced hyperpolarization in response to light onset following RVS (Figure 1B) was also detected in response to drifting rings (Figures 2A and 2B).

A careful examination of SAC responses demonstrated that they shifted in time following RVS, with responses to CF and CP motion shifting in opposite manners. To quantify this, we measured the time of response from stimulus onset (i.e., the response delay). Stimulus onset was set to the time the leading edge of the ring encountered the cell's dendritic arbor (i.e., traversed the most proximal processes for CF motion and the most distal processes for CP motion). To compensate for SAC polarity switch, we measured SAC response delay according to the location of the bright ring in DA conditions and the dark ring following RVS. We found that response delay to CF motion increased on average by 128 ms following RVS ( $\text{delay}_{\text{DA\_CF}} = 49 \pm 52$  ms,  $\text{delay}_{\text{RVS\_CF}} = 177 \pm 53$  ms;  $p < 0.001$ ; Figure 2E), corresponding to the leading-edge location at 43 and 159  $\mu\text{m}$  away from cell soma under DA conditions and following RVS, respectively (Figure 2F, top). For CP motion, the response delay shortened by 59 ms on average following RVS ( $\text{delay}_{\text{DA\_CP}} = 123 \pm 58$  ms,  $\text{delay}_{\text{RVS\_CP}} = 64 \pm 42$  ms;  $p < 0.005$ ; Figure 2E), corresponding to the leading-edge location at 110 and 57  $\mu\text{m}$  away from the cell's distal processes in DA conditions and following RVS, respectively (i.e., 40 and 93  $\mu\text{m}$  from cell soma; Figure 2F, bottom). These spatial measurements are consistent with the observed expansion of SAC receptive field surround. SAC directional responses and phase shifts correlate with their polarity preference (Figures S1D–S1G), suggesting they share a common origin. We previously showed that SAC polarity switch is independent of inhibition (Vlasits et al., 2014). Consistently, blocking GABA-A receptors had no effect on response timing (Figure S2A), and phase shifts detected in SAC voltage responses were also observed in their excitatory input (data not shown). This indicates that excitation, rather than inhibition, underlies the observed polarity switch and the time shift in SAC responses following RVS.

### Center-Surround Reorganization Predicts Loss of CF Preference and Phase Shift in SAC Responses

We tested the role of SACs receptive field organization in their directional responses. First, we used SAC excitatory postsynaptic currents (EPSCs) in response to static rings (Figures 1D and 1E) to simulate SAC response to motion, by shifting responses in time in an orderly manner and summing them (Lien and Scanziani, 2018), either from smallest to largest ring,

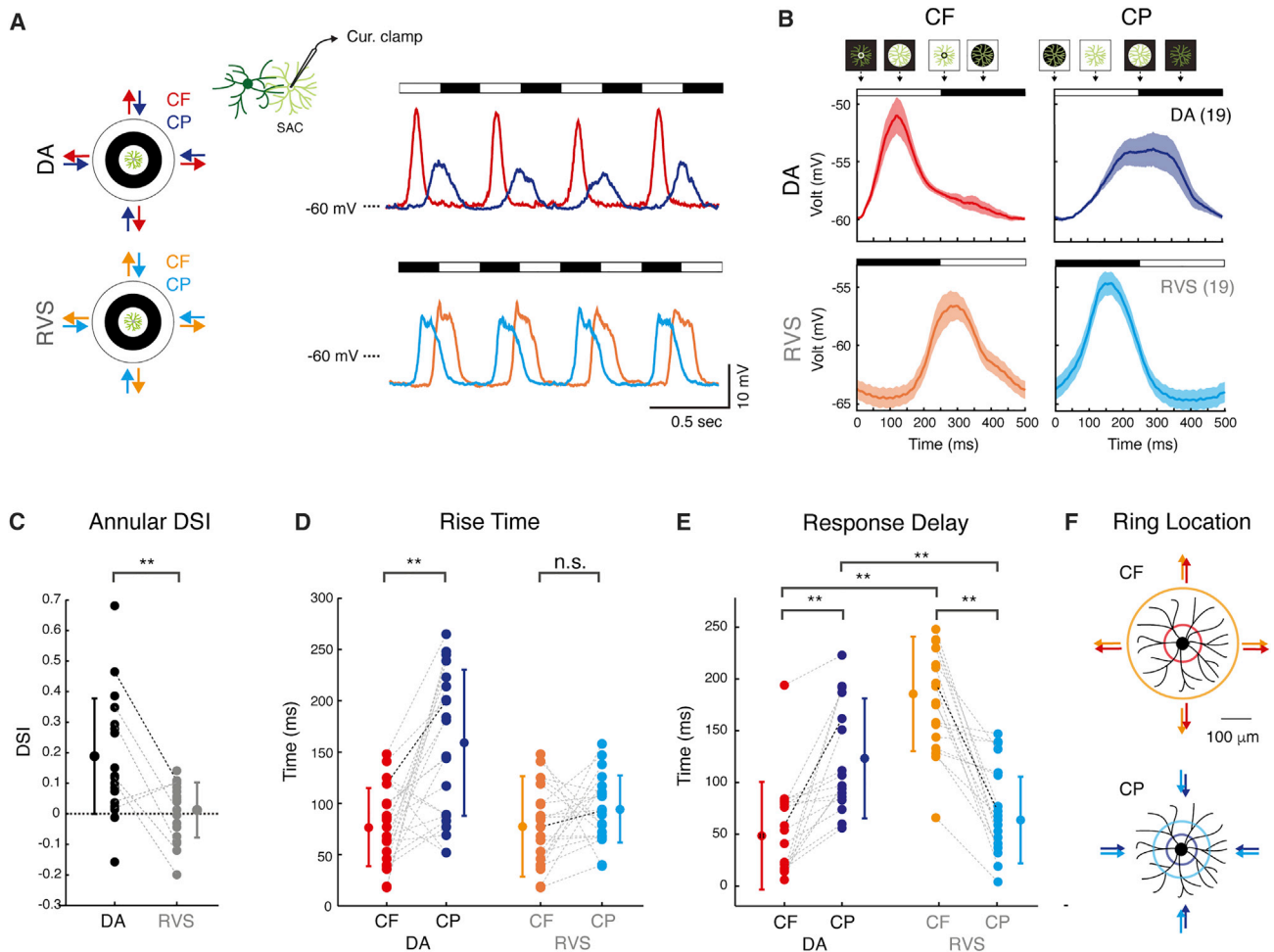


**Figure 2. RVS Abolishes SAC CF Preference and Shifts Its Response Time**

(A) Left: illustration of the stimulus. Right: average current-clamp recordings from an example On-SAC in response to CF and CP motion in DA conditions (top) and following RVS (bottom).

(B) One-cycle waveforms of On-SAC population responses to CF and CP rings (mean  $\pm$  SEM) in DA conditions (top) and following RVS (bottom). Black and white bars denote the ring's location with respect to the SAC processes (proximal and distal processes for CF and CP motion, respectively).

(C) A-DSI of On-SAC population in DA conditions and following RVS.

(D and E) Rise time (D) and response delay (E) of CF and CP motion responses in DA conditions and following RVS.

(F) Colored rings depict the location of the ring's leading edge relative to SAC (white ring for DA, black for RVS) at the time of average response onset depicted in (E). For (C)–(E), group means and SD are indicated on the side by circles and error bars. Bold lines represent the cell in (A). Asterisks indicate statistical significance (\*\* $p < 0.005$ ).

to mimic CF motion, or from largest to smallest ring, to mimic CP motion (Figures S2B–S2E). We set the shifts to fit the velocity of the moving rings. The summation revealed a mild CF preference in DA SACs that disappeared following RVS (Figures 3A and 3B), suggesting that proximal excitation in DA SACs contributes to their CF preference in terms of amplitude and kinetics.

Next, we asked whether changes in SAC receptive field organization can account for the time shift in their responses. For this, we simulated SAC responses to drifting rings in a morphology-based modeling environment (see STAR Methods). The excitatory receptive field of the simulated SAC was set to match the experimental results in each condition (Figures 1D, 1E, and 2F; Figures S1B and S1C): in the DA SAC, excitation was restricted to the proximal

two-thirds of the dendritic arbor, whereas for the RVS SAC, it was distributed along the entire dendritic arbor and stronger in the distal two-thirds processes (Figure 3C). In response to CF motion, the spatial shift of the receptive field caused a delay of  $\sim 70$  ms in depolarization of the post-RVS relative to the DA SAC, whereas in response to CP motion, depolarization of the post-RVS preceded that of the DA SAC by  $\sim 50$  ms (Figure 3D). These trends are in line with the phase shifts observed in our experimental data following RVS. Because SAC release sites are restricted to distal processes (Ding et al., 2016), we extracted the voltage in the distal processes of DA and RVS-simulated SACs and found a comparable shift to the one observed in the somatic voltage (Figure 3E). Hence spatial organization of SAC excitatory

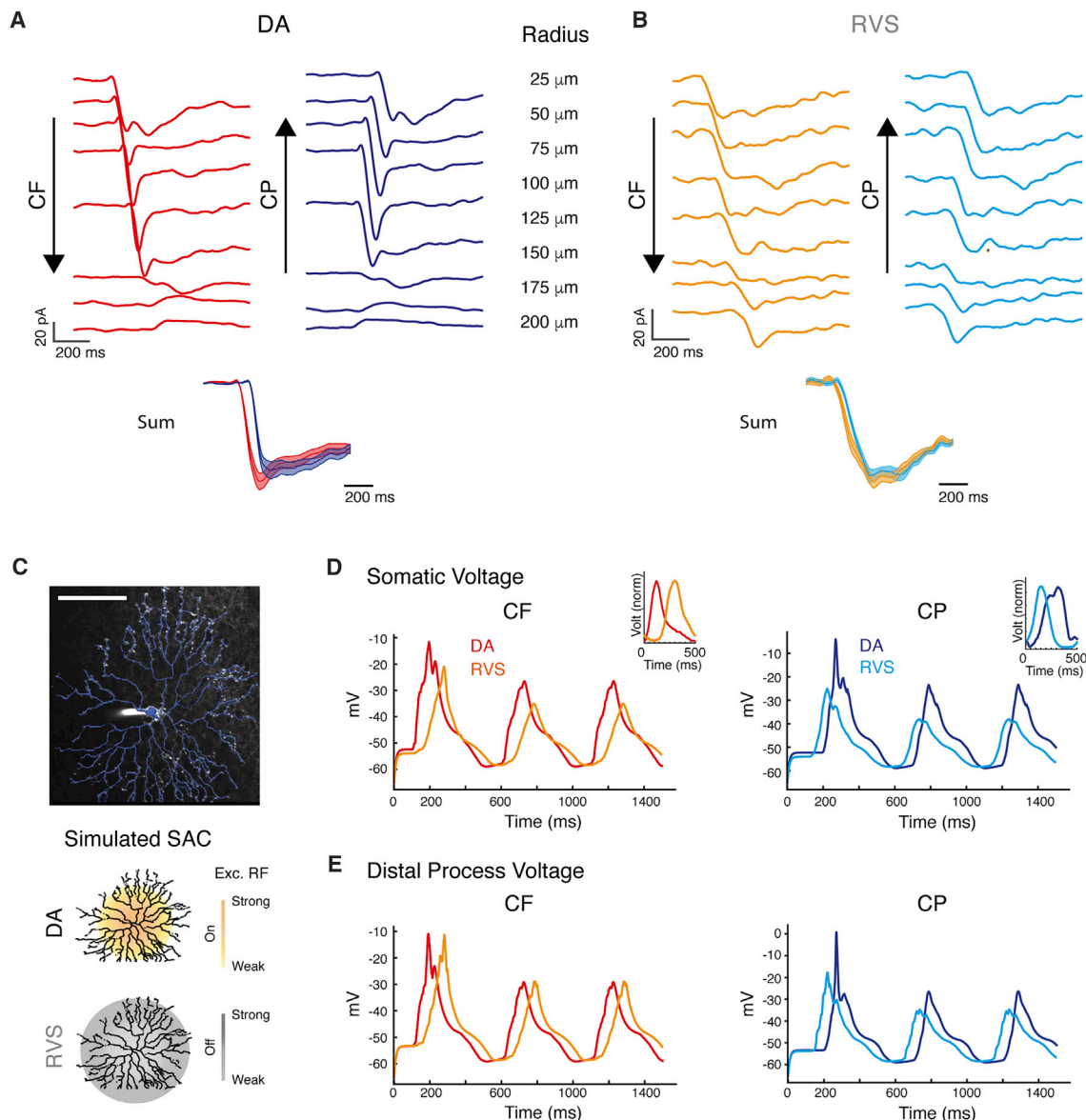


**Figure 3. Models for the Role of Excitatory Receptive Field Organization in SAC Directional Responses**

(A) Population average EPSCs evoked in DA SAC in response to rings of different radii. The traces are shifted in time to simulate proximal-to-distal CF motion (left) and distal-to-proximal CP motion (right). Bottom: linear summation of the shifted responses  $\pm$  SEM (see Figure S2).

(B) As in (A), but for SAC recorded following RVS.

(C) Top: projection of an On-SAC filled with fluorescent dye (white) and its reconstruction (blue). Scale bar: 100  $\mu\text{m}$ . Bottom: schematics of excitatory receptive field, in DA conditions (top, yellow area) and following RVS (bottom, gray area).

(D) Example somatic voltage of a simulated SAC response to CF and CP motion under the two excitatory receptive fields shown in (C). DA traces (red, blue) are plotted on top of RVS traces (orange, cyan). Insets depict the superimposed normalized average responses to CF and CP motion recorded from On-SAC.

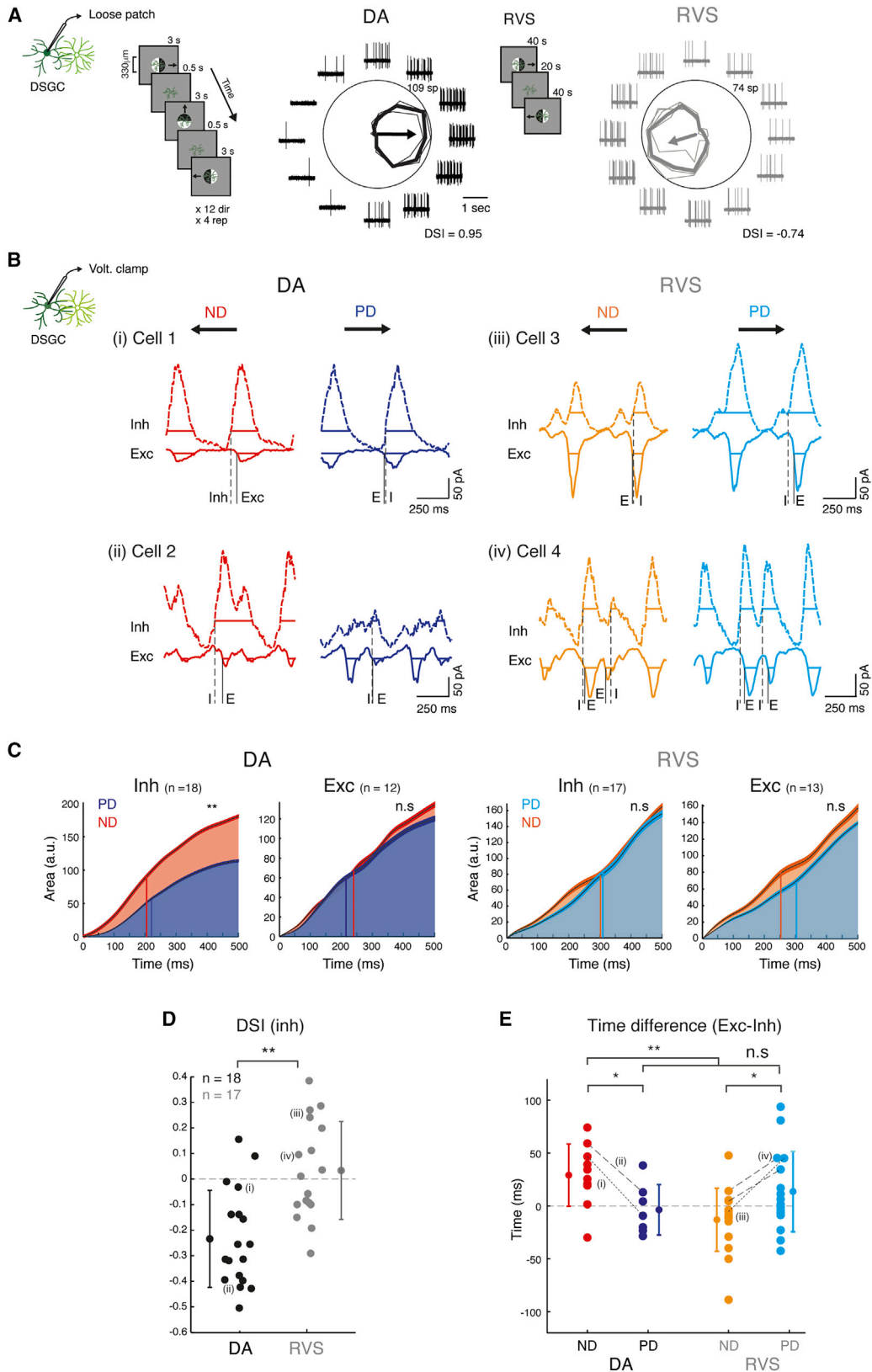
(E) As in (D), but for SAC distal processes ( $d = 135 \mu\text{m}$  from soma).

receptive field predominantly controls the time of its directional response.

### Loss of Directional Preference in SACs Is Reflected in the Inhibitory Inputs to DSGCs

How do changes in SAC receptive field organization affect DSGCs? One may expect that the loss of SAC directional re-

sponses would abolish direction selectivity in DSGCs, but we have previously shown that a subset of DSGCs reverse their directional preference following RVS (Rivlin-Etzion et al., 2012). In the dorsal retina,  $\sim 50\%$  of DSGCs reverse their preference and  $\sim 25\%$  lose their ability to encode motion preference (Figure S1H). To link the changes in SAC responses to DSGCs' reversal, we conducted cell-attached recordings



(legend on next page)

from posterior-preferring On-Off DSGCs. We confirmed reversal of directional preference by measuring DSGC directional tuning in response to linear drifting gratings in DA conditions and following RVS (Figure 4A). We then voltage-clamped DSGCs to record their inhibitory and excitatory inputs in response to gratings. Although few DA DSGCs displayed symmetric inhibition (Figure 4Bi), inhibition tended to be stronger during null than during preferred motion, resulting in negative DSI (Figures 4Bii and 4D;  $DSI_{DA} = -0.23 \pm 0.2$ ). Comparison of the integrated inhibitory inputs over one grating cycle revealed ~30% less total inhibition during preferred than during null motion (Figure 4C, left). Because null motion of a given DSGC corresponds to CF motion in the SAC processes that innervate it, these findings match SAC CF preference. Excitation to DA DSGCs during preferred and null motion was on average equal in size (Figure 4C). Following RVS, inhibitory inputs turned mostly symmetric (Figures 4Biv and 4D;  $DSI_{RVS} = 0.03 \pm 0.2$ ), with a few DSGCs exhibiting an even stronger inhibition in response to motion in the original PD (Figure 4Biii; Rivlin-Etzion et al., 2012). The integrated inhibitory inputs during preferred and null motion were comparable (Figure 4C, right). These changes are in line with the loss of SAC CF preference following RVS, supporting the hypothesis that changes in inhibitory input to DSGCs result from changes in SAC responses following RVS.

### Changes in Timing of Inhibition to DSGCs Can Underlie Reversal of Directional Preference

We investigated whether the RVS-mediated temporal shift in SAC responses underlies the reversal of directional preference in DSGCs in the absence of directional inhibition. First, we compared the time it took evoked inputs to reach half the integrated value under DA conditions and following RVS (Figure 4C). We found that in DA DSGCs, inhibition was ~16 ms faster during null than during preferred motion, whereas excitation was ~25 ms faster during preferred motion. Following RVS, inhibition was slightly faster during original null than during original preferred motion by ~8 ms, but excitation was ~50 ms faster during original null motion. Next, we measured the temporal differences between excitation and inhibition at the single-cell level based on the initial phases of synaptic inputs ( $d = t_{Exc} - t_{Inh}$ ; see STAR Methods). In DA DSGCs, inhibition tended to precede excitation during null, but not preferred, motion ( $d_{ND} = 29 \pm 18$  ms,  $d_{PD} = -4 \pm 24$  ms;  $p < 0.05$ ), whereas following RVS, inhibition tended to precede excitation during original preferred, but not original null, motion ( $d_{PD} = 14 \pm 38$  ms,  $d_{ND} = -13 \pm 30$  ms;  $p <$

0.05; Figures 4B and 4E). The excitation-inhibition temporal balance can account for directional responses in DA DSGCs even in the absence of asymmetric inhibition (e.g., Figure 4Bi), and the shifts in the temporal balance following RVS can account for reversal of directional preference in DSGCs. Indeed, arithmetic summation of excitation and inhibition predicts DSGCs' spike timing and directional preference (Figure S3). These findings suggest that direction selectivity in DSGCs strongly depends on SAC center-surround receptive field organization, which rules both SAC response amplitude and timing.

### DISCUSSION

SAC CF preference is thought to contribute to direction selectivity by providing DSGCs with stronger inhibition during null motion. We found that in the dorsal retina, RVS eliminates On-SAC CF preference and turns inhibition to DSGC symmetric. Despite the loss of SAC directional responses, ~50% of DSGCs reversed their directional preference and ~25% lost their directional preference (Figure S1H). This could result from a shift in SAC response timing that reversed the excitatory-inhibitory balance in DSGCs to support the ND response. We hypothesize that this time shift is due to loss of SAC center and enhancement of surround following RVS (Figure S4). Center-surround receptive fields can dynamically change with visual input (Rivlin-Etzion et al., 2018; Wienbar and Schwartz, 2018), and such deviations were also detected *in vivo* (Sagdu-laev and McCall, 2005). Hence SAC response timing can be adjusted in different contexts, imposing flexibility on the hard-wired direction-selective circuit.

### SACs Mediate Direction Selectivity via Multiple Mechanisms

SAC excitatory inputs were shown to be restricted to its proximal processes, and this distribution is thought to contribute to its CF preference (Ding et al., 2016; Vlasits et al., 2016). Our results support these findings, but also suggest that this proximal excitation can serve DSGC direction selectivity by controlling not only the amount of inhibition but also its timing. During CF motion (corresponding to DSGCs' ND), a response rapidly emerges in DA SACs but arises in delay in RVS-exposed SACs. During CP motion (DSGCs' PD), the response is delayed in DA SACs but arises earlier following RVS. Our experimental and modeling data suggest that this phase shift is mediated by SAC-enhanced surround response following RVS. Thus,

### Figure 4. Temporal Shift of Inhibition Supports Reversal of DSGC's Directional Preference

- (A) An example DSGC directional tuning to drifting gratings (shown on the left) in DA conditions (left) and following RVS (right). RVS is illustrated in the center. Traces are examples of 1-s recordings. Polar plots represent the mean response (spike count during 3 s), and thin lines show the responses in each repetition. Arrows represent the normalized vectorial summation (with outer ring equal to 1).
- (B) Mean voltage clamp recordings of four example DSGCs in response to gratings moving in the PD (blue, cyan) and ND (red, orange) in DA conditions (left) and following RVS (right). Horizontal lines represent the detected response phases, which determine time of response onset (vertical continuous and dashed lines for excitation [E] and inhibition [I], respectively).
- (C) Cumulative current during PD and ND motion of inhibitory and excitatory average normalized waveforms (mean  $\pm$  SEM). Vertical lines denote the time of 50% maximal value (PD: blue and cyan, and ND: red and orange, for DA conditions and following RVS, respectively).
- (D) DSI of inhibition in DA conditions and following RVS.
- (E) Time difference between excitatory and inhibitory response onset during PD and ND motion in DA conditions and following RVS.
- For (D) and (E), group means and SD are indicated on the side by circles and error bars; dashed lines connect values of the cells depicted in (B). Asterisks indicate statistical significance (\* $p < 0.05$ ; \*\* $p < 0.005$ ).

SAC proximal excitation can support direction selectivity via multiple mechanisms.

Whereas the majority of SACs in the dorsal retina switch polarity and lose CF preference following RVS (Figures 1 and 2; Figure S1; Vlasits et al., 2014), about 25% of DSGCs do not change their PD (Figure S1H), implying that additional sources for direction selectivity may be involved (Hanson et al., 2019; Matsumoto et al., 2019; Pei et al., 2015; Percival et al., 2019). Notably, no DSGC reorients its tuning to orthogonal direction (Rivlin-Etzion et al., 2012). Because SAC processes that innervate a DSGC are antiparallel to its PD (Briggman et al., 2011), the phase shift following RVS is maximal along the PD-ND axis, limiting the change in directional preference to 180 degrees and revealing the constraints of dynamic computations in hard-wired neuronal circuits.

DSGCs can preserve their directional preference even upon symmetric inhibition, via inhibition-excitation temporal balance provided by SACs, which corelease GABA and acetylcholine (Hanson et al., 2019). In our experiments, excitation to DSGCs is combination of glutamatergic and cholinergic inputs from bipolar cells and SACs, respectively. The change in SAC response timing following RVS probably shifted the release time of both GABA and acetylcholine. Unlike SAC inhibition, the cholinergic excitation to DSGCs is symmetric (Lee et al., 2010) and is thought to contribute to the computation during grating stimuli (Grzywacz et al., 1998; Huang et al., 2019). The cholinergic input may also cooperate with the GABAergic input to mediate reversal: DSGCs' null motion corresponds to CF motion in null-side SAC processes, resulting in delayed inhibition, but also to CP motion in preferred-side SAC processes, leading to faster cholinergic excitation. Because changes in SAC receptive field organization originate from their excitatory glutamatergic input (Vlasits et al., 2014), bipolar cells that innervate DSGCs are also expected to enhance surround responses and shift their response timing. Yet, the shift in response timing depends on the size of the receptive field, so bipolar cells are expected to display milder shifts than those of SACs, which bear larger dendritic arbors. Thus, temporal relationships between excitation and inhibition are not maintained following RVS, enabling reversal of DSGCs directional preference in the absence of other SAC response asymmetries.

### Similarity and Differences between On and Off Computations of Motion Direction

Here, we focused on On-SACs and how they are affected by RVS. For DSGCs analysis, we pooled On and Off response phases, assuming that On and Off SACs provide a mirror symmetric contribution to direction selectivity. Indeed, both On- and Off-SACs display CF preference and asymmetric wiring to DSGCs (Briggman et al., 2011; Chen et al., 2016; Franssen and Borghuis, 2017). Like On-SACs, Off-SACs were also shown to switch polarity following RVS (Vlasits et al., 2014). Yet, it is possible that the mechanisms implemented by On- and Off-SACs are not fully identical (Wei, 2018). In addition, the temporal proximity in the gratings' On and Off phases may enhance interactions between On and Off pathways (Ackert et al., 2009; Rosa et al., 2016). Thus, a different stimulus with lower spatial frequency should be used to investigate the differential role of On- and Off-SAC in RVS-mediated reversal.

### Center-Surround Antagonism and Polarity Switch in Retinal Cells

Although RVS differs from a simple light adaptation, it is intriguing to note that the polarity switch in SACs is in accordance with surround enhancement at high light levels (Rivlin-Etzion et al., 2018). DSGCs were shown to maintain their PD over a large intensity range (Yao et al., 2018), but the RVS used here was in the high photopic regimen and consisted of drifting gratings, suggesting that a subset of DSGCs can change their directional preference with certain input conditions. Polarity switch in On-SACs does not rely on changes in inhibitory circuits in the inner retina, but rather on opposed polarity activation of presynaptic On bipolar cells (Vlasits et al., 2014). This was suggested to result from loss of rod signaling, because rods are saturated in response to the high-light levels of RVS, serving instead as relay neurons for cone-driven surround inhibition via horizontal cells (Szikra et al., 2014; Vlasits et al., 2014). This cone-mediated surround response is transferred from bipolar cells to SACs and can underlie the polarity switch and the expansion of SAC excitatory receptive fields from center to surround (Figure S4).

### Null-Tuned Directional Response and Antagonistic Surround

According to our data, SAC center and surround stimulation differentially affect SACs' response timing, with temporal characteristics of SAC responses upon surround stimulation resembling those of SAC responses following RVS. This suggests that SAC center-surround organization is a crucial component in determining DSGC directional preference and acts upon it in a PD-center ND-surround antagonistic manner, supporting a response to the PD upon activation of its center, but to the ND upon activation of its surround. In line with this hypothesis, antagonistic center-surround organization for motion encoding was previously described in the optic tectum of pigeons, where the cells' response to motion in the center receptive field was facilitated by motion in the opposite direction in their surround (Frost and Nakayama, 1983). Similar effects were reported for direction-selective cells in the cat superior colliculus and V1, as well as in area MT of primates (Allman et al., 1985; von Grünau and Frost, 1983; Sterling and Wickelgren, 1969; Tanaka et al., 1986). Whether retinal direction selectivity relies on similar motifs requires further investigation, but if true, it implies that dynamic center-surround organization is beneficial for retinal encoding, not only for increasing sensitivity to fine spatial structures but also for sharpening any visual property encoded by retinal ganglion cells, including the computation of motion direction.

### STAR★METHODS

Detailed methods are provided in the online version of this paper and include the following:

- KEY RESOURCES TABLE
- RESOURCE AVAILABILITY
  - Lead Contact
  - Materials Availability
  - Data and Code Availability

- EXPERIMENTAL MODEL AND SUBJECT DETAILS
- METHOD DETAILS
  - Electrophysiological Recordings
  - Light Stimulation
  - Computational Modeling
  - Data Analysis
- QUANTIFICATION AND STATISTICAL ANALYSIS

### SUPPLEMENTAL INFORMATION

Supplemental Information can be found online at <https://doi.org/10.1016/j.celrep.2020.107608>.

### ACKNOWLEDGMENTS

We thank Prof. Marla Feller, Dr. Anna Vlasits, Oren Amsalem, as well as Prof. Ilan Lampl and other members in the Weizmann's Neurobiology department and our lab members for their productive comments on the manuscript. This work was supported by research grants from the European Research Council (ERC starter No. 757732), I-CORE (grant no. 51/11), Israel Science Foundation (1396/15), Minerva Foundation, Dr. and Mrs. Alan Leshner, Lubin-Schupf Fund for Women in Science, Charles and David Wolfson Charitable Trust, Simon Family Foundation, and Lois Pope. L.A. was supported by ISEF. M.R.-E. is the incumbent of the Sara Lee Schupf Family Chair.

### AUTHOR CONTRIBUTIONS

The project was conceived by M.R.-E. and L.A. All physiological experiments were performed by L.A. Analyses were performed by L.A. and M.R.-E. The morphology-based simulation was created by E.E.-T. Validation of the linear model using apparent-motion data was analyzed by S.R.M. N.K. performed genotyping of the transgenic mice and provided other technical support. The manuscript was written and edited by M.R.-E. and L.A. All other authors provided comments during the editing stage.

### DECLARATION OF INTERESTS

The authors declare no competing interests.

Received: October 7, 2019  
Revised: January 22, 2020  
Accepted: April 13, 2020  
Published: May 5, 2020

### SUPPORTING CITATIONS

The following references appear in the Supplemental Information: Gavrikov et al. (2006); Ozaita et al. (2004).

### REFERENCES

Ackert, J.M., Farajian, R., Völgyi, B., and Bloomfield, S.A. (2009). GABA blockade unmasks an OFF response in ON direction selective ganglion cells in the mammalian retina. *J. Physiol.* *587*, 4481–4495.

Allman, J., Miezin, F., and McGuinness, E. (1985). Stimulus specific responses from beyond the classical receptive field: neurophysiological mechanisms for local-global comparisons in visual neurons. *Annu. Rev. Neurosci.* *8*, 407–430.

Barlow, H.B. (1953). Summation and inhibition in the frog's retina. *J. Physiol.* *119*, 69–88.

Briggman, K.L., Helmstaedt, M., and Denk, W. (2011). Wiring specificity in the direction-selectivity circuit of the retina. *Nature* *471*, 183–188.

Chen, Q., Pei, Z., Koren, D., and Wei, W. (2016). Stimulus-dependent recruitment of lateral inhibition underlies retinal direction selectivity. *eLife* *5*, e21053.

Ding, H., Smith, R.G., Poleg-Polsky, A., Diamond, J.S., and Briggman, K.L. (2016). Species-specific wiring for direction selectivity in the mammalian retina. *Nature* *535*, 105–110.

Euler, T., Detwiler, P.B., and Denk, W. (2002). Directionally selective calcium signals in dendrites of starburst amacrine cells. *Nature* *418*, 845–852.

Fransen, J.W., and Borghuis, B.G. (2017). Temporally Diverse Excitation Generates Direction-Selective Responses in ON- and OFF-Type Retinal Starburst Amacrine Cells. *Cell Rep.* *18*, 1356–1365.

Frost, B.J., and Nakayama, K. (1983). Single visual neurons code opposing motion independent of direction. *Science* *220*, 744–745.

Gavrikov, K.E., Nilson, J.E., Dmitriev, A.V., Zucker, C.L., and Mangel, S.C. (2006). Dendritic compartmentalization of chloride cotransporters underlies directional responses of starburst amacrine cells in retina. *Proc. Natl. Acad. Sci. USA* *103*, 18793–18798.

Grzywacz, N.M., Merwine, D.K., and Amthor, F.R. (1998). Complementary roles of two excitatory pathways in retinal directional selectivity. *Vis. Neurosci.* *15*, 1119–1127.

Hanson, L., Sethuramanujam, S., deRosenroll, G., Jain, V., and Awatramani, G.B. (2019). Retinal direction selectivity in the absence of asymmetric starburst amacrine cell responses. *eLife* *8*, e42392.

Haussell, S.E., Euler, T., Detwiler, P.B., and Denk, W. (2007). A dendrite-autonomous mechanism for direction selectivity in retinal starburst amacrine cells. *PLoS Biol.* *5*, e185.

Huang, X., Rangel, M., Briggman, K.L., and Wei, W. (2019). Neural mechanisms of contextual modulation in the retinal direction selective circuit. *Nat. Commun.* *10*, 2431.

Huberman, A.D., Wei, W., Elstrott, J., Stafford, B.K., Feller, M.B., and Barres, B.A. (2009). Genetic identification of an On-Off direction-selective retinal ganglion cell subtype reveals a layer-specific subcortical map of posterior motion. *Neuron* *62*, 327–334.

Koren, D., Grove, J.C.R., and Wei, W. (2017). Cross-compartmental Modulation of Dendritic Signals for Retinal Direction Selectivity. *Neuron* *95*, 914–927.e4.

Kuffler, S.W. (1953). Discharge patterns and functional organization of mammalian retina. *J. Neurophysiol.* *16*, 37–68.

Lee, S., and Zhou, Z.J. (2006). The synaptic mechanism of direction selectivity in distal processes of starburst amacrine cells. *Neuron* *51*, 787–799.

Lee, S., Kim, K., and Zhou, Z.J. (2010). Role of ACh-GABA cotransmission in detecting image motion and motion direction. *Neuron* *68*, 1159–1172.

Lien, A.D., and Scanziani, M. (2018). Cortical direction selectivity emerges at convergence of thalamic synapses. *Nature* *558*, 80–86.

Matsumoto, A., Briggman, K.L., and Yonehara, K. (2019). Spatiotemporally asymmetric excitation supports mammalian retinal motion sensitivity. *Curr. Biol.* *29*, 3277–3288.e5.

Oesch, N.W., and Taylor, W.R. (2010). Tetrodotoxin-resistant sodium channels contribute to directional responses in starburst amacrine cells. *PLoS ONE* *5*, e12447.

Ozaita, A., Petit-Jacques, J., Völgyi, B., Ho, C.S., Joho, R.H., Bloomfield, S.A., and Rudy, B. (2004). A unique role for Kv3 voltage-gated potassium channels in starburst amacrine cell signaling in mouse retina. *J. Neurosci.* *24*, 7335–7343.

Pei, Z., Chen, Q., Koren, D., Giammarinaro, B., Acaron Ledesma, H., and Wei, W. (2015). Conditional Knock-Out of Vesicular GABA Transporter Gene from Starburst Amacrine Cells Reveals the Contributions of Multiple Synaptic Mechanisms Underlying Direction Selectivity in the Retina. *J. Neurosci.* *35*, 13219–13232.

Percival, K.A., Venkataramani, S., Smith, R.G., and Taylor, W.R. (2019). Directional excitatory input to direction-selective ganglion cells in the rabbit retina. *J. Comp. Neurol.* *527*, 270–281.

Poleg-Polsky, A., Ding, H., and Diamond, J.S. (2018). Functional Compartmentalization within Starburst Amacrine Cell Dendrites in the Retina. *Cell Rep.* *22*, 2898–2908.

- Rivlin-Etzion, M., Zhou, K., Wei, W., Elstrott, J., Nguyen, P.L., Barres, B.A., Huberman, A.D., and Feller, M.B. (2011). Transgenic mice reveal unexpected diversity of on-off direction-selective retinal ganglion cell subtypes and brain structures involved in motion processing. *J. Neurosci.* *31*, 8760–8769.
- Rivlin-Etzion, M., Wei, W., and Feller, M.B. (2012). Visual stimulation reverses the directional preference of direction-selective retinal ganglion cells. *Neuron* *76*, 518–525.
- Rivlin-Etzion, M., Grimes, W.N., and Rieke, F. (2018). Flexible neural hardware supports dynamic computations in retina. *Trends Neurosci.* *41*, 224–237.
- Rosa, J.M., Morrie, R.D., Baertsch, H.C., and Feller, M.B. (2016). Contributions of rod and cone pathways to retinal direction selectivity through development. *J. Neurosci.* *36*, 9683–9695.
- Sagdullaev, B.T., and McCall, M.A. (2005). Stimulus size and intensity alter fundamental receptive-field properties of mouse retinal ganglion cells in vivo. *Vis. Neurosci.* *22*, 649–659.
- Singer, J.H., and Diamond, J.S. (2006). Vesicle depletion and synaptic depression at a mammalian ribbon synapse. *J. Neurophysiol.* *95*, 3191–3198.
- Sterling, P., and Wickelgren, B.G. (1969). Visual receptive fields in the superior colliculus of the cat. *J. Neurophysiol.* *32*, 1–15.
- Szikra, T., Trenholm, S., Drinnenberg, A., Jüttner, J., Raics, Z., Farrow, K., Biel, M., Awatramani, G., Clark, D.A., Sahel, J.-A., et al. (2014). Rods in daylight act as relay cells for cone-driven horizontal cell-mediated surround inhibition. *Nat. Neurosci.* *17*, 1728–1735.
- Tanaka, K., Hikosaka, K., Saito, H., Yukie, M., Fukada, Y., and Iwai, E. (1986). Analysis of local and wide-field movements in the superior temporal visual areas of the macaque monkey. *J. Neurosci.* *6*, 134–144.
- Vlasits, A.L., Bos, R., Morrie, R.D., Fortuny, C., Flannery, J.G., Feller, M.B., and Rivlin-Etzion, M. (2014). Visual stimulation switches the polarity of excitatory input to starburst amacrine cells. *Neuron* *83*, 1172–1184.
- Vlasits, A.L., Morrie, R.D., Tran-Van-Minh, A., Bleckert, A., Gainer, C.F., DiGregorio, D.A., and Feller, M.B. (2016). A role for synaptic input distribution in a dendritic computation of motion direction in the retina. *Neuron* *89*, 1317–1330.
- von Grünau, M., and Frost, B.J. (1983). Double-opponent-process mechanism underlying RF-structure of directionally specific cells of cat lateral suprasylvian visual area. *Exp. Brain Res.* *49*, 84–92.
- Warwick, R.A., Kaushansky, N., Sarid, N., Golan, A., and Rivlin-Etzion, M. (2018). Inhomogeneous encoding of the visual field in the mouse retina. *Curr. Biol.* *28*, 655–665.e3.
- Watanabe, D., Inokawa, H., Hashimoto, K., Suzuki, N., Kano, M., Shigemoto, R., Hirano, T., Toyama, K., Kaneko, S., Yokoi, M., et al. (1998). Ablation of cerebellar Golgi cells disrupts synaptic integration involving GABA inhibition and NMDA receptor activation in motor coordination. *Cell* *95*, 17–27.
- Wei, W. (2018). Neural mechanisms of motion processing in the mammalian retina. *Annu. Rev. Vis. Sci.* *4*, 165–192.
- Wienbar, S., and Schwartz, G.W. (2018). The dynamic receptive fields of retinal ganglion cells. *Prog. Retin. Eye Res.* *67*, 102–117.
- Yao, X., Cafaro, J., McLaughlin, A.J., Postma, F.R., Paul, D.L., Awatramani, G., and Field, G.D. (2018). Gap Junctions Contribute to Differential Light Adaptation across Direction-Selective Retinal Ganglion Cells. *Neuron* *100*, 216–228.e6.
- Zhou, Z.J., and Lee, S. (2008). Synaptic physiology of direction selectivity in the retina. *J. Physiol.* *586*, 4371–4376.

## STAR★METHODS

### KEY RESOURCES TABLE

REAGENT or RESOURCE	SOURCE	IDENTIFIER
Chemicals, Peptides, and Recombinant Proteins		
AMES	Vector Laboratories	RRID: IMSR_JAX:030258
SR-95531	Tocris	CAS: 104104-50-9
Experimental Models: Organisms/Strains		
Mouse: <i>mGluR2-EGFP (Gm2-EGFP)</i>	The Jackson Laboratory	RRID: IMSR_JAX:030258
Mouse: <i>TRHR-EGFP</i>	MMRRC	RRID: 030036-UCD
Mouse: <i>DRD4-EGFP</i>	MMRRC	RRID: 000231-UNC
Software and Algorithms		
MATLAB	MathWorks	<a href="https://www.mathworks.com/">https://www.mathworks.com/</a>
pCLAMP 10	Molecular Devices	<a href="https://de.moleculardevices.com/products/axon-patch-clamp-system/acquisition-and-analysis-software/pclamp-software-suite">https://de.moleculardevices.com/products/axon-patch-clamp-system/acquisition-and-analysis-software/pclamp-software-suite</a>
Psychtoolbox-3	N/A	<a href="http://psychtoolbox.org/">http://psychtoolbox.org/</a>
Prairie View	Bruker Technologies	<a href="https://www.bruker.com/products/fluorescence-microscopes/ultima-multiphoton-microscopy/ultima-in-vitro/overview.html">https://www.bruker.com/products/fluorescence-microscopes/ultima-multiphoton-microscopy/ultima-in-vitro/overview.html</a>
NeuroLucida	MBF Bioscience	<a href="https://www.mbfioscience.com/neuroLucida">https://www.mbfioscience.com/neuroLucida</a>
Adobe Illustrator	Adobe	<a href="https://www.adobe.com">https://www.adobe.com</a>
Neuron 7.6	Yale University	<a href="https://neuron.yale.edu/neuron/">https://neuron.yale.edu/neuron/</a>
Python 3.7	N/A	<a href="https://www.python.org/">https://www.python.org/</a>

### RESOURCE AVAILABILITY

#### Lead Contact

Further information and requests for resources should be directed to and will be fulfilled by the Lead Contact, Michal Rivlin-Etzion ([michal.rivlin@weizmann.ac.il](mailto:michal.rivlin@weizmann.ac.il)).

#### Materials Availability

This study did not generate new unique reagents.

#### Data and Code Availability

The datasets and code supporting the current study are available from the corresponding author on request.

### EXPERIMENTAL MODEL AND SUBJECT DETAILS

Two-photon targeted recordings from DSGCs were performed using *Drd4-EGFP* (<https://www.mmrc.org/strains/231/0231.html>) (Huberman et al., 2009) and *Trhr-EGFP* (<https://www.mmrc.org/strains/30036/030036.html>) (Rivlin-Etzion et al., 2011) mice which express GFP in posterior-preferring On-Off DSGCs. Recordings from On-SACs were performed using *mGluR* mice (Watanabe et al., 1998). Pre-weaning animals were housed with their mother; weaned animals were housed in groups of no more than five in individually ventilated cages at 25°C with 12-h light and 12-h dark cycles and free access to food and water. Mice were from either sex, 4-7 weeks old. All procedures were approved by the Institutional Animal Care and Use Committee (IACUC) at the Weizmann Institute of Science.

### METHOD DETAILS

#### Electrophysiological Recordings

Mice were dark-adapted for at least 30 min before isoflurane anesthesia and decapitation. The retina was extracted and dissected in oxygenated Ames medium (Sigma, St. Louis, MO, USA) under dim red and infrared light. The isolated retina (dorsal part) was

then mounted on a 0.22 mm membrane filter (Millipore) with a pre-cut window to allow light to reach the retina and put under a two-photon microscope (Bruker, Billerica, MA, USA) equipped with a Mai-Tai laser (Spectra-physics, Santa Clara, CA, USA) as previously described (Warwick et al., 2018). GFP cells were targeted for recordings with the laser set to 920 nm to minimally activate photoreceptors, and using a 60x water-immersion objective (Olympus, Tokyo, Japan). The isolated retina was perfused with warmed Ames solution (32–34°C) and equilibrated with carbogen (95% O<sub>2</sub>:5% CO<sub>2</sub>).

Spike recordings from DSGCs were made in loose cell-attached mode using 4–7 MΩ glass pipettes filled with Ames solution. Current-clamp recordings from SAC were made using 5–9-MΩ glass pipettes containing (in mM): 110 KCl, 2 NaOH, 2 MgCl<sub>2</sub>, 0.5 CaCl<sub>2</sub>, 5 EGTA, 10 HEPES, 2 ATP, 0.5 GTP and 2 Ascorbate (pH = 7.2 with KOH; Osmolarity = 280). Voltage-clamp whole-cell recordings from SACs and DSGCs were made using 5–9 MΩ glass electrodes filled with intracellular solution containing (in mM): 110 CsMeSO<sub>3</sub>, 2.8 NaCl, 4 EGTA, 20 HEPES, 5 TEA-Cl, 4 Mg-ATP, 0.3 Na<sub>3</sub>GTP, 10 Na<sub>2</sub>-Phosphocreatine and 0.025 AlexaFluor594 (pH = 7.2 with CsOH; Osmolarity = 290; E<sub>Cl</sub> = –73mV). Holding voltages for measuring excitation and inhibition after correction for the liquid junction potential were 0 mV and –60 mV, respectively. For both SACs and DSGCs, we recorded a portion of the cells both before and after RVS, while a portion of the cells was recorded in one condition only. This was done to ensure that effects of RVS do not result from prolonged intracellular recordings. Data were acquired using pCLAMP10, filtered at 2 kHz and digitized at 10 kHz with a MultiClamp 700B amplifier (Molecular Devices, CA, USA) and a Digidata 1550 digitizer (Molecular Devices).

### Light Stimulation

Visual stimuli were generated using MATLAB and the Psychophysics Toolbox and were projected to the retina by a monochromatic organic light-emitting display (OLED-XL, 800 × 600 pixels, 85 Hz refresh rate, eMagin, Bellevue, WA, USA), through either 60x or 20x objectives (UMPLFLN60xW/UMPLFLN20xW; Olympus, Tokyo, Japan). All experiments were carried out in the photopic light range, with a background light intensity of 4.3x10<sup>4</sup> R\*/rod/sec (defined as light off) and a bright light intensity ranging between 4x10<sup>5</sup> and 1x10<sup>6</sup> R\*/rod/sec. Visual stimuli were centered on the recorded cell's soma and focused on the photoreceptor layer. For examination of SAC polarity, a bright spot (50 μm radius) on a dark background was presented to the cell for 2 s. For investigation of SAC receptive field, 8 bright static rings (25 μm width) ranging from 25 to 200 μm radii were centered on cell soma and presented for 2 s each, repeated five times in a pseudo-random order. SAC directional responses were assessed by presentation of expanding (centrifugal; CF) and collapsing (centripetal; CP) rings centered on the SAC soma, projected via the 20x objective for 5 s and repeated five times in a pseudo-random order. The spatial frequency of the rings was 450 μm/cycle, so it contained periods where the SAC processes were fully covered by the bright or by the dark ring (SAC dendritic length from soma is estimated by ~150 μm, and the dark and bright rings are 225 μm width). Temporal frequency of the rings was 2 Hz, resulting in 900 μm/sec. SAC soma was masked by a 25 μm radius gray spot (Euler et al., 2002). First cycle was removed from analysis. DSGC directional responses were assessed from the responses to linear drifting gratings (900 μm/sec, 2 Hz, 450 μm/cycle; first cycle was removed from analysis) in 12 different directions, projected via the 60x objective for 3 s and repeated four times in a pseudo-random order. Repetitive visual stimulation (RVS) consisted of linear gratings (900 μm/sec, 2 Hz, 450 μm/cycle) moving in the preferred and null directions for 40 s and repeated up to 4 times (Rivlin-Etzion et al., 2012).

### Computational Modeling

We reconstructed an individual SAC filled with AlexaFluor594 using NeuroLucida 360 Studio from a three-dimensional volume data acquired using a two-photon microscope (Bruker, Billerica, MA, USA) at 760 nm. Images were acquired at 0.5 μm interval using a 60x objective (UMPLFLN60xW Olympus, Tokyo, Japan). We assumed SAC processes were completely flat and therefore used a projection of the reconstructed SAC. We estimated the diameter of each dendritic region based on its distance from the soma according to values acquired from EM data:  $0.2 \cdot e^{-x/40} + 0.15$  (Poleg-Polsky et al., 2018). The SAC was discretized to 755 segments. To mimic the different excitatory receptive fields, we implanted excitatory inputs in the form of synapses in a semi-random pattern according to a predefined uniform density distribution. For dark-adapted conditions, we restricted excitatory inputs to SACs' proximal 2/3 dendritic arbor (Figures 1D and 1E). Accordingly, synapse density distribution was set to 15% of the sections in the most proximal processes, and gradually decreased (over 20 μm) to reach 10% at 2/3 of the dendritic tree, generating 399 synapses. For post-RVS conditions, excitatory inputs were present along the entire SAC dendritic arbor (Figures 1D and 1E; Figures S1B and S1C). Density distribution was set to 5% of the sections in the proximal 1/3 processes and gradually increased (over 20 μm) to 12% of the sections in the distal processes, generating 758 synapses. Ribbon synapses were modeled using current clamps, each bound to a postsynaptic channel defined by a ligand-activated Markov sequential-state machine, where the ready releasable pool of vesicles was set to 70, generating a maximal post synaptic current of 200 pA, with a 5% probability of release and refilling rate of 4 vesicles per simulation interval (25 ms) (Singer and Diamond, 2006). Membrane ion channels were defined as: R<sub>m</sub> = 10 kΩ/cm<sup>2</sup>; C<sub>m</sub> = 1 μF; R<sub>i</sub> = 75 Ω/cm; V<sub>m</sub> = –60 mV; Channels density (in S/cm<sup>2</sup>): NaV1.8 0.25e<sup>-3</sup>; Kdr at the soma 3e<sup>-3</sup>, 2e<sup>-3</sup> at the processes; L-type Ca<sup>2+</sup> 1e<sup>-3</sup> at the distal 2/3 and zero elsewhere (Ding et al., 2016).

Visual stimuli were introduced to the simulated SAC via the excitatory synapses. This was accomplished by current-clamping a presynaptic compartment that represented each synaptic input according to the spatiotemporal pattern of the stimuli. Visual stimulation resembled the CF and CP moving rings (900 μm/s, 2 Hz, 450 μm/cycle). Simulations were conducted using NEURON

7.6 and run on Intel i9-7900x 3.3GHz 10-core Processor, 64GB RAM and NVIDIA Titan Xp 12GB GPU, with a Linux operating system. Simulated SAC responses were taken from SAC soma. For dendritic voltage measurements we randomly picked a distal process ( $d = 135 \mu\text{m}$  from soma).

### Data Analysis

For DSGC spiking responses, we extracted spike times from the data after offline filtration using a 4 pole Butterworth bandpass filter between 80 and 2000 Hz. The preferred direction of each cell in dark adapted conditions was determined by first normalizing the average spike count in each direction by the total number of spikes for all directions. The vectorial summation of these normalized responses yielded a vector which direction was the preferred direction of the cell and which magnitude gave the width of the tuning (vector sum, ranges between 0 and 1). The direction selective index (DSI) for both DSGC spiking activity and current recordings was calculated as:

$$DSI = \frac{PD_R - ND_R}{PD_R + ND_R} \quad (\text{Equation 1})$$

where  $PD_R$  is the average number of spikes (for DSGC spiking), or the amplitude of the response (for DSGC currents), in the stimulus direction closest to the preferred direction and  $ND_R$  is the average number of spikes (or response amplitude) in the stimulus 180 degrees opposite. In dark adapted conditions DSI values were positive, reaching a maximum of 1 for perfectly tuned DSGC. Following RVS the DSI was calculated based on the original preferred and null directions, resulting in negative values for DSGC which reversed their directional preference. In cells that were recorded only following RVS (i.e., were exposed to RVS before recording started), the preferred direction was set according to at least one dark adapted cell within the same retinal piece which determined the posterior direction of the preparation (assuming all GFP positive cells were tuned to the same posterior direction; Huberman et al., 2009; Rivlin-Etzion et al., 2011).

To assess DSGC response parameters we first averaged for each direction of motion the currents over four repetitions and over cycles, deleting the first cycle (overall 5 cycles, as the stimulus was given at 2 Hz for 3 s). Voltage-clamp raw traces are presented after processing with a Savitzky-Golay filter (3<sup>rd</sup> degree polynomial; window length: 81). Only cells that had either excitation larger than 40 pA or inhibition larger than 70 pA were included in the analysis.

Response phases were detected by threshold crossing, determined as 4 STD above baseline. The STD was calculated by the STD of the PD and ND traces after subtraction of the smoothed traces (Gaussian filter, 60 ms wide), and the baseline was set to the minimum of the average traces. Phases were then sorted by their area under the curve, and only the first three largest phases were considered. From that, we deleted phases shorter than 16 ms. Finally, the data was smoothed with Gaussian filter (to remove any small fluctuations that can be considered as peaks), and we detected peaks in the data. The peaks were not used to determine phase time. Instead, if two peaks were detected within one response phase, the phase was separated into two phases based on the local minimum. The analysis was run on 11 DSGC in the DA conditions and 13 DSGC following RVS. The detection method usually resulted in 0-2 response phases in each average trace, except for 4 traces where 3 phases were detected. We then matched between excitatory and inhibitory phases by pairing each excitatory phase with the closest inhibitory phase. This was determined according to the absolute value of the difference between times of phase onset. Each inhibitory phase could be paired with only one excitatory phase, and only pairs of phases that were less than 100 ms apart were included in the analysis.

To quantify the similarity between DSGCs spiking activity and the voltage clamp recordings (Figure S3), both loose-patch and voltage clamp recordings were performed in DA conditions or following RVS. The excitatory and inhibitory currents were then normalized based on peak response to PD and ND motion, and summed arithmetically. The resulting summation waveform was multiplied by  $-1$  to fix for the negative polarity of excitation, then truncated above 0 to maintain only the positive values of the waveform. To quantify the extent of overlap between the truncated arithmetic summation and spike PSTH, the arithmetic summation was decimated to fit the bin size of the PSTH (10 ms bin) and multiplied by the PSTH values. The percent of overlapping bins was calculated as the number of positive bins in the multiplication vector out of the total number of bins that displayed positive values in the PSTH.

SAC polarity preference was assessed by the On-Off index (OOI):

$$OOI = \frac{On_{amp} - Off_{amp}}{On_{amp} + Off_{amp}} \quad (\text{Equation 2})$$

where  $On_{amp}$  and  $Off_{amp}$  are the amplitudes of the SAC's mean response during a 400 ms time window from 50 ms after light onset and 100 ms after light offset, accordingly (Vlasits et al., 2014). Out of 25 cells recorded in dark adapted conditions 2 cells displayed depolarization in response to both On- and Off-phases (ambiguous cells,  $-0.1 < OOI < 0.1$ ) and were removed from further analysis. Out of 25 cells recorded following RVS, 1 cell maintained its On response and was classified as stable ( $OOI > 0.1$ ). Finally, one On-SAC recorded in voltage clamp mode in dark-adapted conditions was ambiguous and removed from receptive field analysis.

SAC directional tuning was determined by the annular DSI, which was calculated based on equation (1) above, with  $PD_R$  and  $ND_R$  set to the amplitude of the SAC's mean response to CF and CP motion, respectively. To quantify response delay, we assessed the time from stimulus onset to response onset (time the response reached 20% of the response peak). In dark adapted conditions,

we determined the stimulus onset as the time the leading bright edge of the ring encountered the cell's dendritic arbor (i.e., when leading edge traversed most proximal processes for CF motion and most distal processes for CP motion). Following RVS, we used similar measures but in relation to the dark edge of the ring, due to SAC polarity switch. For CF motion, we took into consideration the masking of SAC soma with a 25  $\mu\text{m}$  radius spot (Euler et al., 2002) for determining stimulus onset. Response rise time was calculated as the time from response onset to time of peak response.

Assessing relationships between On-SAC responses to static spots and moving rings stimuli (Figures S1D–S1G) was done by comparing the OOI to either the rise time index or the phase index, calculated as in equation (i) above, with  $PD_R$  and  $ND_R$  set to the SACs' response rise time or response delay during CF and CP motion, respectively.

Simulation of SAC responses to motion is based on their responses to static rings of different radii, where each mean response was shifted in time to simulate motion-induced activation (Lien and Scanziani, 2018). In the dark-adapted condition we set time 0 to 200 ms prior to ring onset, following RVS it was set to 200 ms before ring offset due to polarity switch. To mimic CF motion, responses started with the most proximal ring and ended with the most distal ring, with each consecutive ring response being shifted by additional 27 ms (to mimic  $\sim 900 \mu\text{m}/\text{sec}$  speed). For CP motion, responses started with the most distal ring and ended with the most proximal ring. The shifted waveforms were then summed to mimic the motion response. Validation of the linear model was done using two static rings of different radii (ranging from 50–280  $\mu\text{m}$ ), presented either in isolation or sequentially to generate CF or CP apparent motion (Figures S2C–S2E).

### QUANTIFICATION AND STATISTICAL ANALYSIS

For statistical analysis, datasets were tested for normality using Chi-square goodness of fit test. Datasets that followed normal distribution were compared using a two-sample unpaired or paired Student's t test, according to data structure and Wilcoxon rank sum test was used for abnormally distributed datasets. Throughout the figures, average waveforms are expressed as means  $\pm$  SEM and population statistics are expressed as error bars  $\pm$  STD, unless specified otherwise. Number of cells in each group are denoted in the figures in brackets, asterisks indicate statistical significance (\* $p < 0.05$ ; \*\* $p < 0.005$ ).